

## Article

# Designing High Entropy Bulk Metallic Glass (HE-BMG) by Similar Element Substitution/Addition

Hongyu Ding <sup>1,2,\*</sup>, Hengwei Luan <sup>2</sup> , Hengtong Bu <sup>2</sup>, Hongjie Xu <sup>2</sup> and Kefu Yao <sup>2,\*</sup>

<sup>1</sup> Marine Equipment and Technology Institute, Jiangsu University of Science and Technology, Zhenjiang 212100, China

<sup>2</sup> School of Materials Science and Engineering, Tsinghua University, Beijing 100084, China; luanhengwei6770@163.com (H.L.); bht20@mails.tsinghua.edu.cn (H.B.); xuhongjie@mail.tsinghua.edu.cn (H.X.)

\* Correspondence: dinghongyu2018@just.edu.cn (H.D.); kfyao@tsinghua.edu.cn (K.Y.)

**Abstract:** In this paper, we report that two newly designed high entropy bulk metallic glasses (HE-BMGs),  $\text{Ti}_{20}\text{Hf}_{20}\text{Cu}_{20}\text{Ni}_{20}\text{Be}_{20}$  with a critical diameter of 2 mm, and  $\text{Ti}_{16.7}\text{Zr}_{16.7}\text{Nb}_{16.7}\text{Cu}_{16.7}\text{Ni}_{16.7}\text{Be}_{16.7}$  with a critical diameter of 1.5 mm, can be fabricated by copper mold casting method. These newly developed HE-BMGs exhibited a high fracture strength over 2300 MPa. The glass forming ability and atomic size distribution characteristics of the HE-BMGs are discussed in detail. Moreover, a parameter  $\delta'$  was proposed to evaluate the atomic size distribution characteristics in different HEAs. It showed that this new parameter is closely related to the degree of lattice distortion and phase selection of high-entropy alloys. Adjusting the value of  $\delta'$  parameter by similar element substitution/addition would be beneficial for designing high entropy bulk metallic glasses.

**Keywords:** high entropy alloy; bulk metallic glass; similar element substitution/addition; glass forming ability; lattice distortion



**Citation:** Ding, H.; Luan, H.; Bu, H.; Xu, H.; Yao, K. Designing High Entropy Bulk Metallic Glass (HE-BMG) by Similar Element Substitution/Addition. *Materials* **2022**, *15*, 1669. <https://doi.org/10.3390/ma15051669>

Academic Editor: Filippo Berto

Received: 31 December 2021

Accepted: 15 February 2022

Published: 23 February 2022

**Publisher's Note:** MDPI stays neutral with regard to jurisdictional claims in published maps and institutional affiliations.



**Copyright:** © 2022 by the authors. Licensee MDPI, Basel, Switzerland. This article is an open access article distributed under the terms and conditions of the Creative Commons Attribution (CC BY) license (<https://creativecommons.org/licenses/by/4.0/>).

## 1. Introduction

In the past few decades, bulk metallic glasses (BMGs) [1–9] and high entropy alloys (HEAs) [10–18] have attracted much attention, owing to their unique structure and properties, such as high strength/hardness, good corrosion/wear resistance, etc. Previously, BMGs and HEAs were developed separately in most cases, following different composition design and fabrication routes. While recent studies show that intersections exist between these two domains, namely some HEAs with meticulously designed composition could be made into BMGs, and hence the high entropy bulk metallic glasses (HE-BMGs) were developed [19–41]. An investigation into HE-BMGs is beneficial for understanding the phase formation rules of HEAs and fundamental issues of BMGs, so it is very important to develop more HE-BMGs.

In our previous work, a  $\text{Ti}_{20}\text{Zr}_{20}\text{Cu}_{20}\text{Ni}_{20}\text{Be}_{20}$  HE-BMG with a critical diameter of 3 mm was successfully obtained by copper mold casting method [24]. By introducing Hf as the sixth constituent element,  $\text{Ti}_{16.7}\text{Zr}_{16.7}\text{Hf}_{16.7}\text{Cu}_{16.7}\text{Ni}_{16.7}\text{Be}_{16.7}$  with a critical diameter of 15 mm [25] and a series of  $\text{Ti}_{20}\text{Zr}_{20}\text{Hf}_{20}(\text{Cu}_{20-x}\text{Ni}_x)\text{Be}_{20}$  HE-BMGs with critical diameters of larger than 12 mm was developed [26,27]. These results indicate that similar element substitution/addition is an effective way for developing new HE-BMGs, just the same as traditional BMGs. Since Hf is an element chemically similar to Zr while Nb and Zr are also very close in the periodic table of elements, it is reasonable to suppose that by substituting Zr with Hf, or by adding Nb in the  $\text{Ti}_{20}\text{Zr}_{20}\text{Cu}_{20}\text{Ni}_{20}\text{Be}_{20}$  quinary HEA system, new HE-BMG with good properties can be obtained. Accordingly, two new HEAs, namely  $\text{Ti}_{20}\text{Hf}_{20}\text{Cu}_{20}\text{Ni}_{20}\text{Be}_{20}$  and  $\text{Ti}_{16.7}\text{Zr}_{16.7}\text{Nb}_{16.7}\text{Cu}_{16.7}\text{Ni}_{16.7}\text{Be}_{16.7}$ , were designed to verify this assumption, and their glass-forming ability, atomic size distribution characteristics, lattice distortion, and phase selection rules of HEAs are discussed in detail.

## 2. Experimental

The master alloy ingots with nominal compositions of  $\text{Ti}_{20}\text{Hf}_{20}\text{Cu}_{20}\text{Ni}_{20}\text{Be}_{20}$  and  $\text{Ti}_{16.7}\text{Zr}_{16.7}\text{Nb}_{16.7}\text{Cu}_{16.7}\text{Ni}_{16.7}\text{Be}_{16.7}$  in equal atomic ratio were prepared by arc melting the mixtures of high purity Ti, Hf, Cu, Ni, Zr, Nb plates, and Be granules (purity higher than 99.99 wt.%) within a pure argon gas environment. Cylindrical rods with different diameters were prepared by copper mold injection or suction casting method. Arc melting and casting was conducted on multi-functional high vacuum arc-melting and melt-spinning system, which was produced by SKY Technology Development Corporation, Shenyang, China. The glassy nature of these as-prepared samples was examined by X-ray diffraction (XRD) technique using a Rigaku D/max-RB XRD spectrometry (Rigaku Corporation, Tokyo, Japan) with Cu  $K\alpha$  radiation ( $\lambda = 0.15406$  nm). Thermal properties of the glassy alloys were examined by a Shimadzu DSC-60 differential scanning calorimeter (Shimadzu Corporation, Kyoto, Japan) instrument under the protection of  $\text{N}_2$  gas (flow rate: 50 mL/min). The applied heating rate was set as 20 K/min. The DSC instrument was calibrated with In and Zn standard specimens. The errors are within  $\pm 1$  K. Compression tests with specimens of  $\text{Ø}2 \times 4$  mm and  $\text{Ø}1.5 \times 3$  mm in size were carried out on WDW-100 testing machine (Shanghai Precision Instrument Co., Ltd, Shanghai, China) under a strain rate of  $4 \times 10^{-4} \text{ s}^{-1}$ .

## 3. Results

Figure 1 shows the XRD spectra of the as-cast  $\text{Ti}_{20}\text{Hf}_{20}\text{Cu}_{20}\text{Ni}_{20}\text{Be}_{20}$  and  $\text{Ti}_{16.7}\text{Zr}_{16.7}\text{Nb}_{16.7}\text{Cu}_{16.7}\text{Ni}_{16.7}\text{Be}_{16.7}$  rods with different diameters. No sharp diffraction peak corresponding to the crystalline phase was observed in the  $\text{Ø}2$  mm  $\text{Ti}_{20}\text{Hf}_{20}\text{Cu}_{20}\text{Ni}_{20}\text{Be}_{20}$  and  $\text{Ø}1.5$  mm  $\text{Ti}_{16.7}\text{Zr}_{16.7}\text{Nb}_{16.7}\text{Cu}_{16.7}\text{Ni}_{16.7}\text{Be}_{16.7}$  samples, indicating that they both possess a fully amorphous structure.

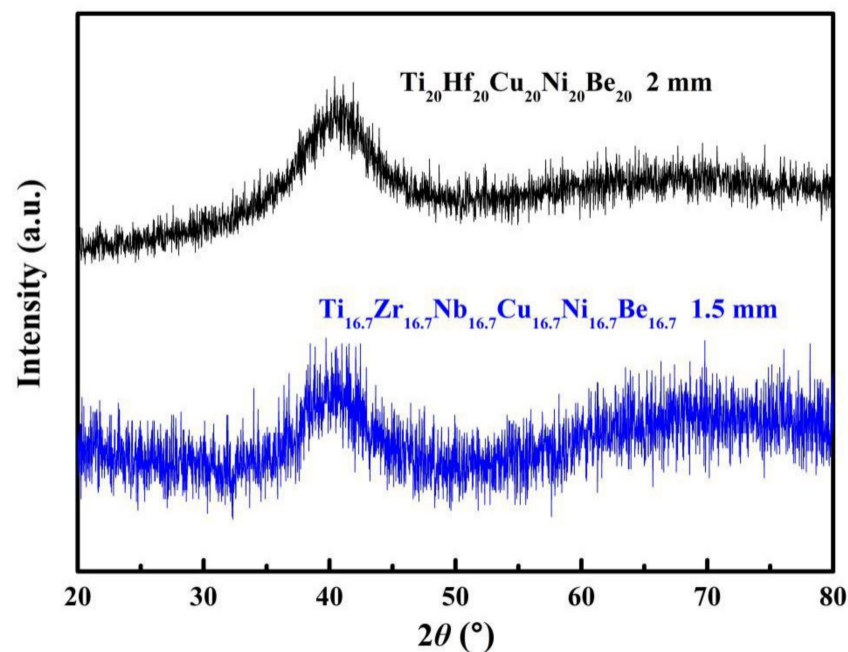


**Figure 1.** XRD spectra of the  $\text{Ø}2$  mm  $\text{Ti}_{20}\text{Hf}_{20}\text{Cu}_{20}\text{Ni}_{20}\text{Be}_{20}$  rod sample and  $\text{Ø}1.5$  mm  $\text{Ti}_{16.7}\text{Zr}_{16.7}\text{Nb}_{16.7}\text{Cu}_{16.7}\text{Ni}_{16.7}\text{Be}_{16.7}$  rod sample.

The DSC curves of the  $\text{Ti}_{20}\text{Hf}_{20}\text{Cu}_{20}\text{Ni}_{20}\text{Be}_{20}$  and  $\text{Ti}_{16.7}\text{Zr}_{16.7}\text{Nb}_{16.7}\text{Cu}_{16.7}\text{Ni}_{16.7}\text{Be}_{16.7}$  samples are shown in Figure 2. The highest test temperature reached 1273 K (1000 °C). However, since the endothermic peak is very high in the high temperature part, glass transition would be very ambiguous in the curve. In order to demonstrate the glass transition phenomenon (which is very important for glasses) clearly, we just cut out temperature less than 1000 K in Figure 2. The glass transition temperature  $T_g$  and initial

crystallization temperature  $T_x$  were marked with arrows.  $T_g$ ,  $T_x$ ,  $T_m$  (melting temperature) and  $T_l$  (liquidus temperature) were measured as 717 K, 760 K, 1095 K, and 1220 K for the  $\text{Ti}_{20}\text{Hf}_{20}\text{Cu}_{20}\text{Ni}_{20}\text{Be}_{20}$  HE-BMG, and 684 K, 739 K, 1066 K, and 1218 K for the  $\text{Ti}_{16.7}\text{Zr}_{16.7}\text{Nb}_{16.7}\text{Cu}_{16.7}\text{Ni}_{16.7}\text{Be}_{16.7}$  HE-BMG, respectively. These data were listed in Table 1.

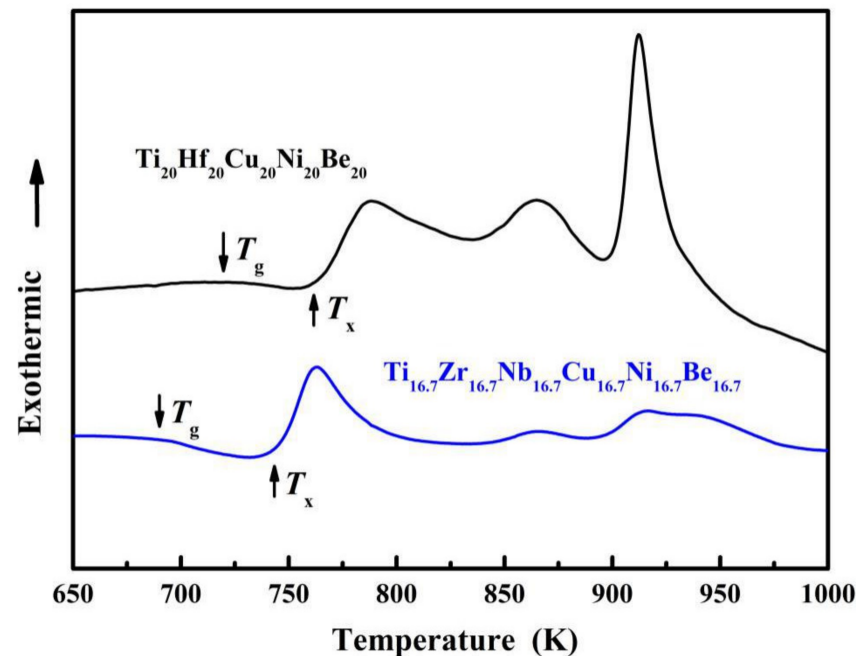
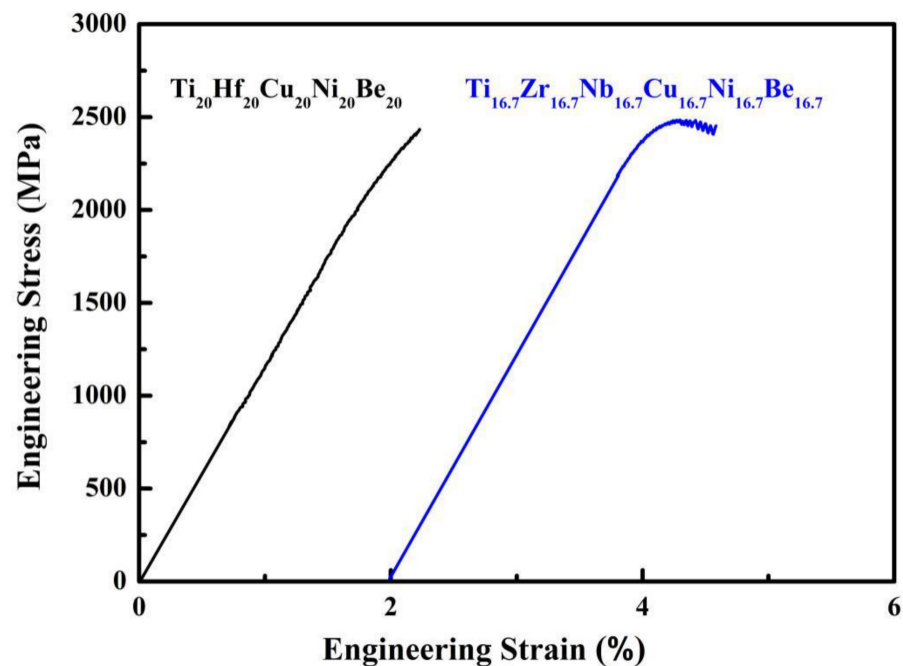


Figure 2. DSC curves of the  $\text{Ti}_{20}\text{Hf}_{20}\text{Cu}_{20}\text{Ni}_{20}\text{Be}_{20}$  and  $\text{Ti}_{16.7}\text{Zr}_{16.7}\text{Nb}_{16.7}\text{Cu}_{16.7}\text{Ni}_{16.7}\text{Be}_{16.7}$  HE-BMGs.

Table 1. Thermal and mechanical properties of some HE-BMGs.

Composition	$T_g$ (K)	$T_x$ (K)	$T_m$ (K)	$T_l$ (K)	$\sigma_{0.2}$ (MPa)	$\sigma_b$ (MPa)	$\epsilon_p$ (%)	Year
$\text{Ti}_{20}\text{Zr}_{20}\text{Cu}_{20}\text{Ni}_{20}\text{Be}_{20}$	683	729	1076	1161	-	2315	0	2013 [24]
$\text{Ti}_{16.7}\text{Zr}_{16.7}\text{Hf}_{16.7}\text{Cu}_{16.7}\text{Ni}_{16.7}\text{Be}_{16.7}$	681	751	1019	1100	1943	2064	0.6	2014 [25]
$\text{Ti}_{20}\text{Hf}_{20}\text{Cu}_{20}\text{Ni}_{20}\text{Be}_{20}$	717	760	1095	1220	-	2425	0	This work
$\text{Ti}_{16.7}\text{Zr}_{16.7}\text{Nb}_{16.7}\text{Cu}_{16.7}\text{Ni}_{16.7}\text{Be}_{16.7}$	684	739	1066	1218	2330	2450	0.5	This work

The stress strain curves of  $\text{Ø}2 \times 4$  mm  $\text{Ti}_{20}\text{Hf}_{20}\text{Cu}_{20}\text{Ni}_{20}\text{Be}_{20}$  and  $\text{Ø}1.5 \times 3$  mm  $\text{Ti}_{16.7}\text{Zr}_{16.7}\text{Nb}_{16.7}\text{Cu}_{16.7}\text{Ni}_{16.7}\text{Be}_{16.7}$  HE-BMG samples in uniaxial compression test were shown in Figure 3. The fracture strength  $\sigma_b$  was 2425 MPa for  $\text{Ti}_{20}\text{Hf}_{20}\text{Cu}_{20}\text{Ni}_{20}\text{Be}_{20}$  HE-BMG, the yield strength  $\sigma_{0.2}$ , fracture strength  $\sigma_b$  and plasticity  $\epsilon_p$  were 2330 MPa, 2450 MPa and 0.5% for  $\text{Ti}_{16.7}\text{Zr}_{16.7}\text{Nb}_{16.7}\text{Cu}_{16.7}\text{Ni}_{16.7}\text{Be}_{16.7}$  HE-BMG, respectively, which were also listed in Table 1. The specimens fractured in a shear mode. It is interesting to note that both  $\text{Ti}_{20}\text{Hf}_{20}\text{Cu}_{20}\text{Ni}_{20}\text{Be}_{20}$  and  $\text{Ti}_{20}\text{Zr}_{20}\text{Cu}_{20}\text{Ni}_{20}\text{Be}_{20}$  quinary HE-BMGs fractured without any plasticity [24], while  $\text{Ti}_{16.7}\text{Zr}_{16.7}\text{Nb}_{16.7}\text{Cu}_{16.7}\text{Ni}_{16.7}\text{Be}_{16.7}$  and  $\text{Ti}_{16.7}\text{Zr}_{16.7}\text{Hf}_{16.7}\text{Cu}_{16.7}\text{Ni}_{16.7}\text{Be}_{16.7}$  senary HE-BMGs exhibited a compressive plasticity of about 0.5%, as well as serration behavior [25]. The reason of this difference remains unclear.



**Figure 3.** Stress strain curves of the  $\text{Ti}_{20}\text{Hf}_{20}\text{Cu}_{20}\text{Ni}_{20}\text{Be}_{20}$  and  $\text{Ti}_{16.7}\text{Zr}_{16.7}\text{Nb}_{16.7}\text{Cu}_{16.7}\text{Ni}_{16.7}\text{Be}_{16.7}$  HE-BMGs.

#### 4. Discussion

##### 4.1. Glass Forming Ability (GFA) of High Entropy Alloys by Element Addition/Substitution

The parameters of supercooled liquid region  $\Delta T$  ( $= T_x - T_g$ ), reduced glass transition temperature  $T_{rg}$  ( $= T_g/T_1$ ), and  $\gamma$  parameter ( $= T_x/(T_g + T_1)$ ) are calculated as 43 K, 0.588, and 0.392 for  $\text{Ti}_{20}\text{Hf}_{20}\text{Cu}_{20}\text{Ni}_{20}\text{Be}_{20}$ , while 55 K, 0.562, and 0.388 for  $\text{Ti}_{16.7}\text{Zr}_{16.7}\text{Nb}_{16.7}\text{Cu}_{16.7}\text{Ni}_{16.7}\text{Be}_{16.7}$ , respectively. Compared with  $\text{Ti}_{20}\text{Zr}_{20}\text{Cu}_{20}\text{Ni}_{20}\text{Be}_{20}$  alloy (3 mm), the critical diameter of  $\text{Ti}_{20}\text{Hf}_{20}\text{Cu}_{20}\text{Ni}_{20}\text{Be}_{20}$ , alloy (2 mm) and  $\text{Ti}_{16.7}\text{Zr}_{16.7}\text{Nb}_{16.7}\text{Cu}_{16.7}\text{Ni}_{16.7}\text{Be}_{16.7}$  (1.5 mm) both decreased. It is noticed that by substitution Zr with Hf, although  $T_{rg}$  remains the same,  $\Delta T$  and  $\gamma$  decreased; by addition of Nb as the sixth element, both  $T_{rg}$  and  $\gamma$  decreased, although  $\Delta T$  increased [24]. It implies that the parameter  $\gamma$  is better than  $T_{rg}$  and  $\Delta T$  in judging the GFA in these high-entropy glassy alloys; meanwhile high entropy is not always beneficial to the GFA of the HEAs. The substitution of element Hf and the addition of Nb brings the liquidus temperature  $T_1$  higher than that of  $\text{Ti}_{20}\text{Zr}_{20}\text{Cu}_{20}\text{Ni}_{20}\text{Be}_{20}$  alloy [24]. As a result, the GFA of the HEA was slightly deteriorated. On the other hand, by the addition of Hf as the sixth element, liquidus temperature  $T_1$  was lowered down. Therefore, the GFA of the  $\text{Ti}_{16.7}\text{Zr}_{16.7}\text{Hf}_{16.7}\text{Cu}_{16.7}\text{Ni}_{16.7}\text{Be}_{16.7}$  was greatly improved as compared with  $\text{Ti}_{20}\text{Zr}_{20}\text{Cu}_{20}\text{Ni}_{20}\text{Be}_{20}$  alloy [25]. These results indicate that lowering down liquidus temperature would be helpful for enhancing the GFA.

##### 4.2. Atomic Radius Characteristics of HE-BMG

The atomic size distribution characteristics of existing HE-BMGs were shown in Table 2. Based on the atomic radius of constituent elements, they were divided into five categories, namely super large atom ( $r > 0.165$  nm), large atom ( $r \approx 0.16$  nm), medium atom ( $r \approx 0.14$  nm), small atom ( $r \approx 0.12$  nm), and ultra-small atom ( $r < 0.12$  nm). It is noticed that most HE-BMGs were comprised of 3 to 4 categories, except for those containing nonmetal element such as Si, P, B, C, etc [29,33,36]. In high entropy alloys, larger atomic radius difference leads to larger lattice distortion. In case that lattice distortion exceeds some degree, the lattice collapse and amorphous structure formed accordingly. This is in agreement with Zhang's work [13].

**Table 2.** Atomic size distribution characteristics of existing HE-BMGs.

Composition	Super Large Atom $r > 0.165$ nm	Large Atom $r \approx 0.16$ nm	Medium Atom $r \approx 0.14$ nm	Small Atom $r \approx 0.12$ nm	Ultra Small Atom $r < 0.12$ nm	Year
Ti <sub>20</sub> Zr <sub>20</sub> Hf <sub>20</sub> Cu <sub>20</sub> Ni <sub>20</sub>		Zr, Hf	Ti	Cu, Ni		2002 [19]
Sr <sub>20</sub> Ca <sub>20</sub> Yb <sub>20</sub> Mg <sub>20</sub> Zr <sub>20</sub>	Sr, Ca, Yb	Mg	Zn			2011 [20,23]
Er <sub>20</sub> Tb <sub>20</sub> Dy <sub>20</sub> Ni <sub>20</sub> Al <sub>20</sub>	Tb, Dy, Er		Al	Ni		2011 [21]
Pd <sub>20</sub> Pt <sub>20</sub> Cu <sub>20</sub> Ni <sub>20</sub> P <sub>20</sub>			Pt, Pd	Cu, Ni	P	2011 [22]
Ti <sub>20</sub> Zr <sub>20</sub> Cu <sub>20</sub> Ni <sub>20</sub> Be <sub>20</sub>		Zr	Ti	Cu, Ni	Be	2013 [24]
Ti <sub>16.7</sub> Zr <sub>16.7</sub> Hf <sub>16.7</sub> Cu <sub>16.7</sub> Ni <sub>16.7</sub> Be <sub>16.7</sub>		Zr, Hf	Ti	Cu, Ni	Be	2014 [25]
Ti <sub>20</sub> Zr <sub>20</sub> Hf <sub>20</sub> (Cu <sub>20-x</sub> Ni <sub>x</sub> )Be <sub>20</sub>		Zr, Hf	Ti	Cu, Ni	Be	2015 [26,27]
Ho <sub>20</sub> Er <sub>20</sub> Co <sub>20</sub> Al <sub>20</sub> Dy <sub>20</sub>	Dy, Ho, Er		Al	Co		2015 [28]
Fe <sub>25</sub> Co <sub>25</sub> Ni <sub>25</sub> (B, Si) <sub>25</sub>				Co, Ni, Fe	Si, B	2015 [29]
Zr <sub>40</sub> Hf <sub>10</sub> Ti <sub>4</sub> Y <sub>1</sub> Al <sub>10</sub> Cu <sub>25</sub> Ni <sub>7</sub> Co <sub>2</sub> Fe <sub>1</sub>	Y	Zr, Hf	Ti, Al	Cu, Co, Ni, Fe		2015 [30]
Er <sub>18</sub> Gd <sub>18</sub> Y <sub>20</sub> Al <sub>24</sub> Co <sub>20</sub>	Y, Gd, Er		Al	Co		2018 [31]
Er <sub>20</sub> Dy <sub>20</sub> Co <sub>20</sub> Al <sub>20</sub> RE <sub>20</sub> (RE = Gd, Tb, Tm)	Gd/Tb, Dy, Er	Tm	Al	Co		2018 [32]
Fe <sub>25</sub> Co <sub>25</sub> Ni <sub>25</sub> (P <sub>0.4</sub> C <sub>0.2</sub> B <sub>0.2</sub> Si <sub>0.2</sub> ) <sub>25</sub>				Co, Ni, Fe	Si, P, B, C	2018 [33]
La <sub>25-35</sub> Ce <sub>25-35</sub> Ni <sub>5-15</sub> Cu <sub>5-15</sub> Al <sub>20</sub>	La, Ce		Al	Cu, Ni		2018 [34]
Fe <sub>25</sub> Co <sub>25</sub> Ni <sub>25</sub> Mo <sub>5</sub> P <sub>10</sub> B <sub>10</sub>			Mo	Co, Ni, Fe	P, B	2019 [35]
(Fe <sub>1/3</sub> Co <sub>1/3</sub> Ni <sub>1/3</sub> ) <sub>80</sub> (P <sub>1/2</sub> B <sub>1/2</sub> ) <sub>20</sub>				Co, Ni, Fe	P, B	2019 [36]
Zr <sub>35</sub> Hf <sub>17.5</sub> Ti <sub>5.5</sub> Al <sub>12.5</sub> Co <sub>7.5</sub> Ni <sub>12</sub> Cu <sub>10</sub>		Zr, Hf	Ti, Al	Cu, Co, Ni		2019 [37]
Gd <sub>25</sub> Co <sub>25</sub> Al <sub>25</sub> Y <sub>15</sub> RE <sub>10</sub> (RE = Dy, Ho, Er)	Y, Gd, (Dy, Ho, Er)		Al	Co		2020 [38]
Fe <sub>20-35</sub> Ni <sub>20</sub> Cr <sub>20-30</sub> Mo <sub>5-15</sub> (P <sub>0.6</sub> C <sub>0.2</sub> B <sub>0.2</sub> ) <sub>20</sub>			Mo	Cr, Ni, Fe	P, B, C	2020 [39]
(Gd <sub>0.2</sub> Dy <sub>0.2</sub> Er <sub>0.2</sub> Co <sub>0.2</sub> Al <sub>0.2</sub> ) <sub>99.5</sub> Si <sub>0.5</sub>	Gd, Dy, Er		Al	Co	Si	2021 [40]
Zr <sub>33</sub> Hf <sub>8</sub> Ti <sub>6</sub> Cu <sub>32</sub> Ni <sub>10</sub> Co <sub>5</sub> Al <sub>6</sub>		Zr, Hf	Ti, Al	Cu, Co, Ni		2021 [41]
Ti <sub>20</sub> Hf <sub>20</sub> Cu <sub>20</sub> Ni <sub>20</sub> Be <sub>20</sub>		Hf	Ti	Cu, Ni	Be	This work
Ti <sub>16.7</sub> Zr <sub>16.7</sub> Nb <sub>16.7</sub> Cu <sub>16.7</sub> Ni <sub>16.7</sub> Be <sub>16.7</sub>		Zr	Ti, Nb	Cu, Ni	Be	This work

#### 4.3. Assessing Degree of Lattice Distortion in High Entropy Alloys by Parameter $\delta'$

The phase formation rule in HEA is of great importance both scientifically and technologically. The formed phase(s) in HEAs (solid solution, intermetallics and amorphous phase) at certain conditions (alloy composition, preparation method, service environment, etc.) remain unknown for most HEAs [10,13,15,18,42]. Many researchers proposed various criteria to solve this problem, such as the  $\delta$ - $\Delta H_{\text{mix}}$  diagram proposed by Zhang et al. [13], VEC criteria proposed by Guo et al. [15], electronegativity mismatch  $D_c$  proposed by Toda-Caraballo et al. [43], etc. Lattice distortion is a crucial factor in HEAs, and it is also very important in determining phase formation. However, the relationship between lattice distortion and phase formation is still not clear. Much research has been devoted to characterizing the degree of lattice distortion, and to further illustrate its correlation with phase formation, such as the  $\gamma$  parameter proposed by Wang et al. [44], the  $\alpha_2$  parameter proposed by Wang et al. [45], etc. However, it is far from clearly understanding. Further investigation is still required.

It is noticed from Table 2 that in most HE-BMGs, the atomic radius of the constituent elements atomic sizes distribute in a wide range; while for many solid solution forming HEAs, atomic sizes are more concentrated (especially for CuCoCrNiFe [10] and Cantor alloy [11], they both possess FCC structure, meanwhile atomic size difference of the constituent elements are very small). However, this is a qualitative description, and it is somehow ambiguous. As a result, a quantitative exemplification is needed.

Based on Table 2, here we propose a new parameter  $\delta'$  to assess the degree of lattice distortion in HEAs. Supposing that a HEA contains N elements, the atomic fractions are  $c_1, c_2 \dots \dots c_N$ , respectively, and the atomic radii are  $r_1, r_2 \dots \dots r_N$  ( $r_1 < r_2 < \dots \dots < r_N$ ), respectively (data from ref. [46]). Then, the average atomic size is defined as  $\bar{r}$ :

$$\bar{r} = \sum_{i=1}^N c_i r_i \quad (1)$$

The lattice distortion parameter  $\delta'$  is defined as

$$\delta' = 100 \sum_1^{N-1} \frac{c_{i+1} + c_i}{2} \frac{r_{i+1} - r_i}{\bar{r}} \quad (2)$$

In particular, for equal atomic alloy,  $\delta'$  is given as

$$\delta' = \frac{100}{N} \frac{r_N - r_1}{\bar{r}} \quad (3)$$

According to Formula (2), lattice distortion parameter  $\delta'$  for some typical HEAs were calculated and listed in Table 3. For clarity, the relationship between atomic size distribution, lattice distortion parameter  $\delta'$ , and phase selection is demonstrated in Figure 4. It is noticed that  $\delta'$  is closely related to phase selection in HEAs: when atomic size difference is relatively small,  $\delta'$  is also small ( $\delta' < 2.2$ ), FCC solid solution would be formed; when the atomic size difference became larger,  $\delta'$  increased, FCC + BCC solid solution would tend to form as  $2.2 < \delta' < 2.9$ ; with even larger  $\delta'$  ( $2.9 < \delta' < 4.9$ ), BCC solid solution would be formed; amorphous phase would be formed as  $\delta'$  exceeds 4.9.

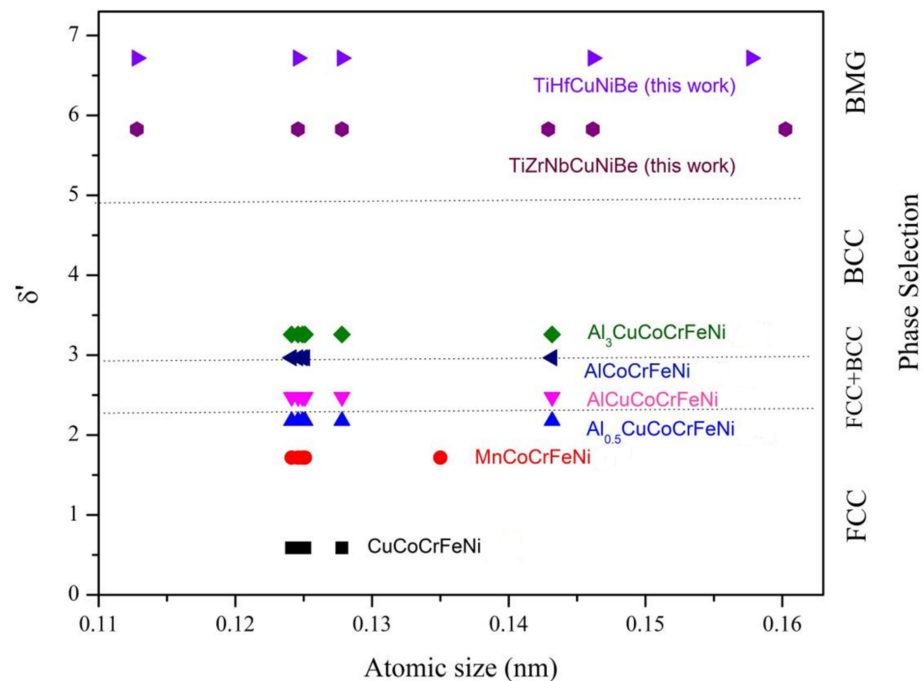


**Figure 4.** Correlation between atomic size distribution, lattice distortion degree parameter  $\delta'$  and phase selection in some typical HEAs [10–12].

The parameter  $\delta'$  can be understood from the point of view of dense atomic packing. Since it is correlated with the degree of lattice distortion, when  $\delta'$  was small, dense random packing FCC phase formed (its density is about 74% for monolic element); with the increase of lattice distortion,  $\delta'$  became larger, looser BCC phase (density of about 68% for monolic element) appeared, and its concentration increased accordingly; when lattice distortion became even serious, lattice collapse and amorphous phase would form eventually. Then, adjusting the lattice distortion or the parameter  $\delta'$  of HEAs, such as by similar element substitution or addition, could be helpful in designing high-entropy metallic glasses.

The new parameter  $\delta'$  we proposed here is somewhat similar with the  $\delta$  parameter proposed by Zhang et al. [13]; it is also affected by the number, type, and concentration of the elements, while its value is smaller than  $\delta$ , as is demonstrated in Table 3. As compared with  $\delta$ ,  $\delta'$  is more sensitive to addition/substitution of an ultra large/small atom. Taking alloy 11 and 12 in Table 3 for example, it can be seen that by substituting Hf element with

much smaller Be element in the Ti-Zr-Hf-Cu-Ni HEA,  $\delta$  increased from 10.324 to 12.514, the growth rate is 21%; while  $\delta'$  increased from 4.977 to 7.065, the growth rate is 42%, much larger than that of  $\delta$ . It indicates that the new parameter  $\delta'$  is more sensitive than  $\delta$  in certain circumstance.

Additionally, it is noticed from Formula (3), for equiatomic high entropy alloys, as the number of elements N increased,  $\delta'$  decreased and lattice distortion is mitigated accordingly. As a result, it is not beneficial for amorphous phase formation, especially for  $N > 10$ . This is in consistent with Cantor's result that an alloy with 16 to 20 elements in equiatomic concentration does not form amorphous phase [11].

**Table 3.** Correlation between atomic size distribution, lattice distortion and phase selection in some typical HEAs.

No.	Composition	$r > 0.165$ nm	$r \approx 0.16$ nm	$r \approx 0.14$ nm	$r \approx 0.12$ nm	$r < 0.12$ nm	$\bar{r}$	$\delta$ [13]	$\delta'$	VEC [15]	Phase
1	CrMnFeCoNi			Mn	Co, Cr, Ni, Fe		1.26744	3.267	1.717	8	FCC [11]
2	CuCoCrNiFe				Cu, Co, Cr, Ni, Fe		1.25304	1.031	0.587	8.8	FCC [10]
3	Al <sub>0.3</sub> CuCoCrFeNi			Al	Cu, Co, Cr, Ni, Fe		1.26315	3.416	2.042	8.472	FCC [10]
4	A <sub>0.5</sub> lCuCoCrFeNi			Al	Cu, Co, Cr, Ni, Fe		1.26928	4.161	2.178	8.273	FCC [10]
5	Al <sub>0.8</sub> CuCoCrFeNi			Al	Cu, Co, Cr, Ni, Fe		1.27768	4.912	2.363	8	FCC + BCC [10]
6	AlCuCoCrFeNi			Al	Cu, Co, Cr, Ni, Fe		1.28281	5.271	2.475	7.833	FCC + BCC [10]
7	Al <sub>2.5</sub> CuCoCrFeNi			Al	Cu, Co, Cr, Ni, Fe		1.31259	6.466	3.106	6.867	FCC + BCC [10]
8	Al <sub>2.8</sub> CuCoCrFeNi			Al	Cu, Co, Cr, Ni, Fe		1.31717	6.554	3.201	6.718	BCC [10]
9	Al <sub>3.0</sub> CuCoCrFeNi			Al	Cu, Co, Cr, Ni, Fe		1.32004	6.598	3.259	6.625	BCC [10]
10	AlCoCrFeNi			Al	Co, Cr, Ni, Fe		1.28378	5.767	2.968	7.2	BCC [12]
11	Ti <sub>20</sub> Zr <sub>20</sub> Hf <sub>20</sub> Cu <sub>20</sub> Ni <sub>20</sub>		Zr, Hf	Ti	Cu, Ni		1.43308	10.324	4.977	-	BMG [19]
12	Ti <sub>20</sub> Zr <sub>20</sub> Cu <sub>20</sub> Ni <sub>20</sub> Be <sub>20</sub>		Zr	Ti	Cu, Ni	Be	1.34318	12.514	7.065	-	BMG [24]
13	Ti <sub>16.7</sub> Zr <sub>16.7</sub> Hf <sub>16.7</sub> Cu <sub>16.7</sub> Ni <sub>16.7</sub> Be <sub>16.7</sub>		Zr, Hf	Ti	Cu, Ni	Be	1.38223	12.773	5.721	-	BMG [25]
14	Ti <sub>20</sub> Hf <sub>20</sub> Cu <sub>20</sub> Ni <sub>20</sub> Be <sub>20</sub>		Hf	Ti	Cu, Ni	Be	1.33818	11.993	6.718	-	BMG (this work)
15	Ti <sub>16.7</sub> Zr <sub>16.7</sub> Nb <sub>16.7</sub> Cu <sub>16.7</sub> Ni <sub>16.7</sub> Be <sub>16.7</sub>		Zr	Ti, Nb	Cu, Ni	Be	1.35495	11.546	5.826	-	BMG (this work)

## 5. Conclusions

In this paper, two new high entropy bulk metallic glasses (HE-BMGs) have been successfully fabricated using copper mold casting method, namely Ti<sub>20</sub>Hf<sub>20</sub>Cu<sub>20</sub>Ni<sub>20</sub>Be<sub>20</sub> with a critical diameter of 2 mm and Ti<sub>16.7</sub>Zr<sub>16.7</sub>Nb<sub>16.7</sub>Cu<sub>16.7</sub>Ni<sub>16.7</sub>Be<sub>16.7</sub> with a critical diameter of 1.5 mm. These two HE-BMGs exhibit high fracture strength over 2300 MPa. The glass forming ability and atomic size distribution characteristics of the HE-BMGs

are discussed, and it is found that atomic radius spans over a wide range in HE-BMGs. Moreover, we propose a new parameter  $\delta'$  to assess the degree of lattice distortion in high entropy alloys (HEAs). It emphasizes the difference between atoms with adjacent atomic size, and it is closely related to phase selection in HEAs. When  $\delta'$  is relatively small ( $\delta' < 2.2$ ), FCC solid solution formed; when  $2.2 < \delta' < 2.9$ , FCC + BCC phases formed; when  $2.9 < \delta' < 4.9$ , BCC phase formed; while  $\delta' > 4.9$ , amorphous phase would be formed. This new parameter  $\delta'$  is beneficial for understanding lattice distortion and phase selection in HEAs. The present work suggests that through adjusting the parameter  $\delta'$  by similar element substitution/addition, that is, adjusting the lattice distortion, is an effective way for designing high entropy bulk glassy alloy.

**Author Contributions:** Conceptualization, H.D.; Data curation, H.X.; Formal analysis, H.L.; Funding acquisition, H.D. and K.Y.; Investigation, H.B.; Methodology, H.B.; Project administration, K.Y.; Software, H.X.; Validation, H.X.; Visualization, H.L.; Writing—Original draft, H.D.; Writing—review & editing, H.L., H.B. and K.Y. All authors have read and agreed to the published version of the manuscript.

**Funding:** This research was funded by the National Key Basic Research and Development Program (Grant No. 2016YFB00300500), National Natural Science Foundation of China (Grant Nos. 51571127 and 51871129). and Youth Fund of Jiangsu Natural Science Foundation (Grant No. BK20190979).

**Institutional Review Board Statement:** Not applicable.

**Informed Consent Statement:** Not applicable.

**Data Availability Statement:** The data that support the plots within this paper and other findings of this study are available from the corresponding authors upon reasonable request.

**Conflicts of Interest:** The authors declare no competing interests. We declare that we have no financial and personal relationships with other people or organizations that can inappropriately influence our work.

## References

1. Greer, A.L. Metallic glasses. *Science* **1995**, *267*, 1947–1953. [[CrossRef](#)] [[PubMed](#)]
2. Johnson, W.L. Bulk glass-forming metallic alloys: Science and technology. *MRS Bull.* **1999**, *24*, 42–56. [[CrossRef](#)]
3. Inoue, A. Stabilization of metallic supercooled liquid and bulk amorphous alloys. *Acta Mater.* **2000**, *48*, 279–306. [[CrossRef](#)]
4. Wang, W.H.; Dong, C.; Shek, C.H. Bulk metallic glasses. *Mater. Sci. Eng. R* **2004**, *44*, 45–89. [[CrossRef](#)]
5. Inoue, A.; Takeuchi, A. Recent development and applications of bulk glassy alloys. *Int. J. Appl. Glass Sci.* **2010**, *1*, 273–295. [[CrossRef](#)]
6. Wang, W.H. The elastic properties, elastic models and elastic perspectives of metallic glasses. *Prog. Mater. Sci.* **2012**, *57*, 487–656. [[CrossRef](#)]
7. Greer, A.L. Metallic glasses. *Phys. Metall.* **2014**, *35*, 305–385. [[CrossRef](#)]
8. Li, H.X.; Lu, Z.C.; Wang, S.L.; Wu, Y.; Lu, Z.P. Fe-based bulk metallic glasses: Glass formation, fabrication, properties and applications. *Prog. Mater. Sci.* **2019**, *103*, 235–318. [[CrossRef](#)]
9. Yang, C.; Zhang, C.; Chen, Z.J.; Li, Y.; Yan, W.Y.; Yu, H.B.; Liu, L. Three-dimensional hierarchical porous structures of metallic glass/copper composite catalysts by 3D printing for efficient wastewater treatments. *ACS Appl. Mater. Inter.* **2021**, *13*, 7227–7237. [[CrossRef](#)]
10. Yeh, J.W.; Chen, S.K.; Lin, S.J.; Gan, J.Y.; Chin, T.S.; Shun, T.T.; Tsau, C.H.; Chang, S.Y. Nanostructured high-entropy alloys with multiple principle elements: Novel alloy design concepts and outcomes. *Adv. Eng. Mater.* **2004**, *6*, 299–303. [[CrossRef](#)]
11. Cantor, B.; Chang, I.; Knight, P.; Vincent, A. Microstructural development in equiatomic multicomponent alloys. *Mater. Sci. Eng. A* **2004**, *375–377*, 213–218. [[CrossRef](#)]
12. Zhou, Y.J.; Zhang, Y.; Wang, Y.L.; Chen, G.L. Solid solution alloys of AlCoCrFeNiTi<sub>x</sub> with excellent room-temperature mechanical properties. *Appl. Phys. Lett.* **2007**, *90*, 181904. [[CrossRef](#)]
13. Zhang, Y.; Zhou, Y.J.; Lin, J.P.; Chen, G.L.; Liaw, P.K. Solid-solution phase formation rules for multi-component alloys. *Adv. Eng. Mater.* **2008**, *10*, 534–538. [[CrossRef](#)]
14. Senkov, O.N.; Wilks, G.B.; Miracle, D.B.; Chuang, C.P.; Liaw, P.K. Refractory high-entropy alloys. *Intermetallics* **2010**, *18*, 1758–1765. [[CrossRef](#)]
15. Guo, S.; Ng, C.; Lu, J.; Liu, C.T. Effect of valence electron concentration on stability of fcc or bcc phase in high entropy alloys. *J. Appl. Phys.* **2011**, *109*, 103505. [[CrossRef](#)]
16. Gludovatz, B.; Hohenwarter, A.; Catoor, D.; Chang, E.H.; George, E.P.; Ritchie, R.O. A fracture-resistant high-entropy alloy for cryogenic applications. *Science* **2014**, *345*, 1153–1158. [[CrossRef](#)]

17. Lu, Y.P.; Dong, Y.; Guo, S.; Jiang, L.; Kang, H.J.; Wang, T.M.; Wen, B.; Wang, Z.J.; Jie, J.C.; Cao, Z.Q.; et al. A promising new class of high-temperature alloys: Eutectic high-entropy alloys. *Sci. Rep.* **2014**, *4*, 6200. [[CrossRef](#)]
18. Ye, Y.F.; Wang, Q.; Lu, J.; Liu, C.T.; Yang, Y. Design of high entropy alloys: A single-parameter thermodynamic rule. *Scr. Mater.* **2015**, *104*, 53–55. [[CrossRef](#)]
19. Ma, L.Q.; Wang, L.M.; Zhang, T.; Inoue, A. Bulk Glass Formation of Ti–Zr–Hf–Cu–M (M = Fe, Co, Ni) Alloys. *Mater. Trans.* **2002**, *43*, 277–280. [[CrossRef](#)]
20. Zhao, K.; Xia, X.X.; Bai, H.Y.; Zhao, D.Q.; Wang, W.H. Room temperature homogeneous flow in a bulk metallic glass with low glass transition temperature. *Appl. Phys. Lett.* **2011**, *98*, 141913. [[CrossRef](#)]
21. Gao, X.Q.; Zhao, K.; Ke, H.B.; Ding, D.W.; Wang, W.H.; Bai, H.Y. High mixing entropy bulk metallic glasses. *J. Non-Cryst. Solids* **2011**, *357*, 3557–3560. [[CrossRef](#)]
22. Takeuchi, A.; Chen, N.; Wada, T.; Yokoyama, Y.; Kato, H.; Inoue, A.; Yeh, J.W. Pd<sub>20</sub>Pt<sub>20</sub>Cu<sub>20</sub>Ni<sub>20</sub>P<sub>20</sub> high-entropy alloy as a bulk metallic glass in the centimeter. *Intermetallics* **2011**, *19*, 1546–1554. [[CrossRef](#)]
23. Li, H.F.; Xie, X.H.; Zhao, K.; Wang, Y.B.; Zheng, Y.F.; Wang, W.H.; Qin, L. In vitro and in vivo studies on biodegradable CaMgZnSrYb high-entropy bulk metallic glass. *Acta Biomater.* **2013**, *9*, 8561–8573. [[CrossRef](#)] [[PubMed](#)]
24. Ding, H.Y.; Yao, K.F. High entropy Ti<sub>20</sub>Zr<sub>20</sub>Cu<sub>20</sub>Ni<sub>20</sub>Be<sub>20</sub> bulk metallic glass. *J. Non-Cryst. Solids* **2013**, *364*, 9–12. [[CrossRef](#)]
25. Ding, H.Y.; Shao, Y.; Gong, P.; Li, J.F.; Yao, K.F. A senary TiZrHfCuNiBe high entropy bulk metallic glass with large glass-forming ability. *Mater. Lett.* **2014**, *125*, 151–153. [[CrossRef](#)]
26. Zhao, S.F.; Yang, G.N.; Ding, H.Y.; Yao, K.F. A quinary Ti-Zr-Hf-Be-Cu high entropy bulk metallic glass with a critical size of 12 mm. *Intermetallics* **2015**, *61*, 47–50. [[CrossRef](#)]
27. Zhao, S.F.; Shao, Y.; Liu, X.; Chen, N.; Ding, H.Y.; Yao, K.F. Pseudo-quinary Ti<sub>20</sub>Zr<sub>20</sub>Hf<sub>20</sub>Be<sub>20</sub>(Cu<sub>20-x</sub>Ni<sub>x</sub>) high entropy bulk metallic glasses with large glass forming ability. *Mater. Des.* **2015**, *87*, 625–631. [[CrossRef](#)]
28. Huo, J.T.; Huo, L.S.; Men, H.; Wang, X.M.; Inoue, A.; Wang, J.Q.; Chang, C.T.; Li, R.W. The magnetocaloric effect of Gd-Tb-Dy-Al-M (M = Fe, Co and Ni) high-entropy bulk metallic glasses. *Intermetallics* **2015**, *58*, 31–35. [[CrossRef](#)]
29. Qi, T.L.; Li, Y.H.; Takeuchi, A.; Xie, G.Q.; Miao, H.T.; Zhang, W. Soft magnetic Fe<sub>25</sub>Co<sub>25</sub>Ni<sub>25</sub>(B, Si)<sub>25</sub> high entropy bulk metallic glasses. *Intermetallics* **2015**, *66*, 8–12. [[CrossRef](#)]
30. Chen, C.; Pang, S.J.; Cheng, Y.Y.; Zhang, T. A centimeter-size Zr<sub>40</sub>Hf<sub>10</sub>Ti<sub>4</sub>Y<sub>1</sub>Al<sub>10</sub>Cu<sub>25</sub>Ni<sub>7</sub>Co<sub>2</sub>Fe<sub>1</sub> bulk metallic glass with high mixing entropy designed by multi-substitution. *J. Non-Cryst. Solids* **2015**, *410*, 39–42. [[CrossRef](#)]
31. Kim, J.; Oh, H.S.; Kim, J.; Ryu, C.W.; Lee, G.W.; Chang, H.J.; Park, E.S. Utilization of high entropy alloy characteristics in Er-Gd-Y-Al-Co high entropy bulk metallic glass. *Acta Mater.* **2018**, *155*, 350–361. [[CrossRef](#)]
32. Li, J.; Xue, L.; Yang, W.M.; Yuan, C.C.; Huo, J.T.; Shen, B.L. Distinct spin glass behavior and excellent magnetocaloric effect in Er<sub>20</sub>Dy<sub>20</sub>Co<sub>20</sub>Al<sub>20</sub>RE<sub>20</sub> (RE = Gd, Tb and Tm) high-entropy bulk metallic glasses. *Intermetallics* **2018**, *96*, 90–93. [[CrossRef](#)]
33. Xu, Y.Q.; Li, Y.H.; Zhu, Z.W.; Zhang, W. Formation and properties of Fe<sub>25</sub>Co<sub>25</sub>Ni<sub>25</sub>(P, C, B, Si)<sub>25</sub> high-entropy bulk metallic glasses. *J. Non-Cryst. Solids* **2018**, *487*, 60–64. [[CrossRef](#)]
34. Wu, L.; Zhao, Y.; Li, J.J.; Wu, J.L.; Zhang, B. Correlation between mechanical and thermodynamic properties for La–Ce–Ni–Cu–Al high-entropy metallic glasses. *J. Iron Steel Res. Int.* **2018**, *25*, 658–665. [[CrossRef](#)]
35. Wu, K.N.; Liu, C.; Li, Q.; Huo, J.T.; Li, M.C.; Chang, C.T.; Sun, Y.F. Magnetocaloric effect of Fe<sub>25</sub>Co<sub>25</sub>Ni<sub>25</sub>Mo<sub>5</sub>P<sub>10</sub>B<sub>10</sub> high-entropy bulk metallic glass. *J. Magn. Magn. Mater.* **2019**, *489*, 165404. [[CrossRef](#)]
36. Li, C.Z.; Li, Q.; Li, M.C.; Chang, C.T.; Li, H.X.; Dong, Y.Q.; Sun, Y.F. New ferromagnetic (Fe<sub>1/3</sub>Co<sub>1/3</sub>Ni<sub>1/3</sub>)<sub>80</sub>(P<sub>1/2</sub>B<sub>1/2</sub>)<sub>20</sub> high entropy bulk metallic glass with superior magnetic and mechanical properties. *J. Alloys Compd.* **2019**, *791*, 947–951. [[CrossRef](#)]
37. Wada, T.; Jiang, J.; Yubuta, K.; Kato, H.; Takeuchi, A. Septenary Zr–Hf–Ti–Al–Co–Ni–Cu high-entropy bulk metallic glasses with centimeter-scale glass-forming ability. *Materialia* **2019**, *7*, 100372. [[CrossRef](#)]
38. Pang, C.M.; Chen, L.; Xu, H.; Guo, W.; Lv, Z.W.; Huo, J.T.; Cai, M.J.; Shen, B.L.; Wang, X.L.; Yuan, C.C. Effect of Dy, Ho, and Er substitution on the magnetocaloric properties of Gd-Co-Al-Y high entropy bulk metallic glasses. *J. Alloys Compd.* **2020**, *827*, 154101. [[CrossRef](#)]
39. Li, Y.H.; Wang, S.W.; Wang, X.W.; Yin, M.L.; Zhang, W. New FeNiCrMo(P, C, B) high-entropy bulk metallic glasses with unusual thermal stability and corrosion resistance. *J. Mater. Sci. Technol.* **2020**, *43*, 32–39. [[CrossRef](#)]
40. Shao, L.L.; Wang, Q.Q.; Xue, L.; Zhu, M.Y.; Wang, A.D.; Luan, J.H.; Yin, K.B.; Luo, Q.; Zeng, Q.S.; Sun, L.T.; et al. Effects of minor Si addition on structural heterogeneity and glass formation of GdDyErCoAl high-entropy bulk metallic glass. *J. Mater. Res. Technol.* **2021**, *11*, 378–391. [[CrossRef](#)]
41. Jalali, A.; Malekan, M.; Park, E.S.; Rashidi, R.; Bahmani, A.; Yoo, G.H. Thermal behavior of newly developed Zr<sub>33</sub>Hf<sub>8</sub>Ti<sub>6</sub>Cu<sub>32</sub>Ni<sub>10</sub>Co<sub>5</sub>Al<sub>6</sub> high-entropy bulk metallic glass. *J. Alloys Compd.* **2021**, *892*, 162220. [[CrossRef](#)]
42. Luan, H.W.; Shao, Y.; Li, J.F.; Mao, W.L.; Han, Z.D.; Shao, C.L.; Yao, K.F. Phase stabilities of high entropy alloys. *Scr. Mater.* **2020**, *179*, 40–44. [[CrossRef](#)]
43. Toda-Caraballo, I.; Rivera-Diaz-del-Castillo, P.E.J. A criterion for the formation of high entropy alloys based on lattice distortion. *Intermetallics* **2016**, *71*, 76–87. [[CrossRef](#)]
44. Wang, Z.J.; Huang, Y.H.; Yang, Y.; Wang, J.C.; Liu, C.T. Atomic-size effect and solid solubility of multicomponent alloys. *Scr. Mater.* **2015**, *94*, 28–31. [[CrossRef](#)]

- 
45. Wang, Z.J.; Qiu, W.F.; Yang, Y.; Liu, C.T. Atomic-size and lattice-distortion effects in newly developed high-entropy alloys with multiple principal elements. *Intermetallics* **2015**, *64*, 63–69. [[CrossRef](#)]
  46. Senkov, O.N.; Miracle, D.B. Effect of the atomic size distribution on glass forming ability of amorphous metallic alloys. *Mater. Res. Bull.* **2001**, *36*, 2183–2198. [[CrossRef](#)]